JOURNAL OF THEORETICAL AND APPLIED MECHANICS
62, 4, pp. 695-711, Warsaw 2024
https://doi.org/10.15632/jtam-pl/193523

DESIGN OF A SEMI-ACTIVE SUSPENSION CONTROL METHOD BASED ON AN ENHANCED INVERSE MODEL FOR NONLINEAR MAGNETORHEOLOGICAL DAMPERS

Lei Jia, Chun Wang
School of Mechanical Engineering, Shenyang Ligong University, Shenyang, China
corresponding author C. Wang, e-mail: wangchun016050@163.com

Yang Tian
School of Mechanical Engineering, Liaoning Engineering Vocational College, Tieling, China

Jiankang Yang, Ziliang Liu, Xin Zhang
School of Mechanical Engineering, Shenyang Ligong University, Shenyang, China

The nonlinear hysteresis characteristics of magnetorheological dampers lead to low fitting accuracy and poor practicality of their inverse models. Hence, to improve the accuracy of an inverse model generated with BP neural network, this research presents a novel optimization approach called Beluga Whale Optimization. The prediction accuracy of current is enhanced by the optimized inverse model. Under the enhanced inverse model, a variable universe fuzzy PID control is created. Based on the research outcomes, it has been shown that the introduction of control contributes to noteworthy improvements in the suspension performance metrics, both in terms of time and frequency domains.

Keywords: semi-active suspension, BP neural network, beluga whale optimization, variable universe fuzzy PID, magnetorheological damper

1. Introduction

The suspension of a vehicle plays a crucial role in minimizing the effects of road vibrations and ensuring stability of the vehicle body (Tseng and Hrovat, 2015). The passive suspension cannot satisfy the needs for complex operating conditions due to its simple structure and fixed parameters, so the intelligent suspension (active suspension, semi-active suspension) has emerged as a hot topic of research (Na *et al.*, 2022; Krzyzynski and Maciejewski, 2019). The active suspension mostly uses the target forces generated by the actuator to cut down vibration. Semi-active suspension has gained considerable attention as an alternative to address the challenges of complexity, exorbitant costs, and excessive energy consumption associated with active suspensions (Liu *et al.*, 2022).

Magnetorheological dampers (MRD) are widely employed intelligent devices for damping vibrations in various fields. They were first introduced into the suspension system by Lou *et al.* (1994), which has aroused the attention of researchers. MRD is a device that uses the magnetorheological effect to control the damping force. MRD offers fast responsiveness, wide control range and low energy consumption, but it also has a powerful hysteresis and nonlinearity. Designing a semi-active suspension control has made it crucial to develop a highly precise MRD model. Consequently, establishing this model has emerged as one of the utmost essential objectives (Mai *et al.*, 2020; Dong *et al.*, 2010). The range of mechanical models has been presented by the researchers (Chen, 2022), including the Bingham model, the Bouc-wen model, and others. The frequent utilization of the Bouc-Wen model (Tang *et al.*, 2020; Gong and Hen, 2020) has been observed to describe the properties of MRD. Boada *et al.* (2018) and Maciejewski *et al.* (2019)

developed an inverse model to output the control current. Zhang and Zhao (2017) has built the inverse model with the BP neural network (BPNN), which output a fairly accurate predicted currents but still had some defects. Ma *et al.* (2021) obtained a higher accurate system with the Elman neural network compared to BPNN. BWO, a bio-inspired optimization technique created by Zhong *et al.* (2022), is applied to tackle challenging engineering and optimization issues. In this paper, the BPNN is optimized to provide a more accurate inverse model thanks to the benefit that the BWO can ensure the algorithm converge globally.

Effective and reasonable control algorithm is another crucial role of the intelligent suspension system for vibration reduction. Successful implementations have been carried out for vibration control of vehicles using control methods such as skyhook control and PID control (Papaioannou *et al.*, 2021; Shin *et al.*, 2016), but semi-active control still faces a huge challenge for the nonlinear characteristics of MRD. The issue at hand has garnered heightened interest in the implementation of nonlinear control techniques, namely fuzzy control, sliding model control, H_∞ control, and neural network control in MRD semi-active suspension systems. This approach aims to address and mitigate the aforementioned challenge (Al Aela *et al.*, 2022). Morales *et al.* (2018) proposed a variable damping control strategy for a semi-active suspension system to improve smoothness of the vehicle ride. As well as compared to other control methods, fuzzy control as an intelligent control can handle many problems that cannot be accurately mathematically modeled in complex systems. Trikande *et al.* (2018) set up a quarter suspension system with fuzzy acceleration and velocity of the suspension. According to the experimental results, it has been shown that the incorporation of fuzzy control significantly improves the stability and ride comfort of the suspension system. In this study, in the realm of active suspension systems, Na *et al.* (2020) introduced an innovative and dynamic approach to regulate control strategies. This scheme effectively ensures vehicle stability in the presence of suspension parameter uncertainties and time delays. Despite the fuzzy control has small overshoot, good robustness and strong adaptability, there is inevitable steady-state control error. Henceforth, merging the concept of fuzzy control with other control approaches becomes imperative in order to obtain optimal control with utmost stability and precision. A fuzzy control strategy for the active suspension in vehicles was introduced by Wang *et al.* (2015). The proposal garnered significant attention as it addresses the issue of balancing control precision and speed, while also confronting the impact of uncertain control parameters. According to the work of Muthalif *et al.* (2017), a semi-active suspension system model was created with integrating fuzzy PID control, where the objective was to enhance control performance by applying fuzzy logic to manipulate the input variables, including body speed and acceleration. Fuzzy PID control not only tackles the issue of steady-state error in control systems, but also provides adaptive adjustment of PID control parameters. Although these aforementioned techniques greatly enhance the precision and adaptability of suspension control, they primarily focus on addressing the uncertainty inherent within their own parameters. As such, they fail to incorporate external excitations and are unable to proactively pre-adjust control parameters to promptly react to variations in external stimuli. In an effort to improve control precision of the fuzzy controller, Pang *et al.* (2018) put forward a variable universe fuzzy T-S with a semi-active suspension system, whereas Zhang *et al.* (2024) designed variable universe fuzzy PID (VUF-PID) for a continuous damping semi-active suspension. The conventional fuzzy PID technique is unable to scale owing to variation of the initial theoretical domain error, causing the system control accuracy decline. The VUF-PID strategy has the advantages of the conventional fuzzy PID, and meanwhile, the utilization rate of fuzzy rules is largely enhanced by adjusting theoretical domain factor, which enhances the system accuracy. The major contribution of this work is a new inverse model of MRD, which estimates the current required to make the desired force exerted by MRD. Prior studies have suggested that the use of fuzzy PID in the suspension system offers considerable robustness. In this study, the notion of variable domains is incorporated into the realm of fuzzy control. By modifying the control

domain, both the controller input and output can be flexibly tailored, thereby enhancing the system adaptability and the performance of the suspension.

Structural organization of the paper is a follows: Section 2 describes the semi-active suspension and MRD dynamic model, Section 3 focuses on design of the MRD inverse model and system controller, Section 4 performs an experimental simulation of the developed controller, and Section 5 provides a summary of the entire work accomplished.

2. Dynamic modeling

2.1. Semi-active suspension system

The vertical force and vibration are the main factors affecting the vehicle suspension system, and the single suspension system mainly responds to vertical motion of the vehicle, so it can fulfill the requirement of the research. This paper focuses on the two-degrees of freedom semi--active suspension system of a quarter vehicle model, which is shown as a simplified model in Fig. 1.

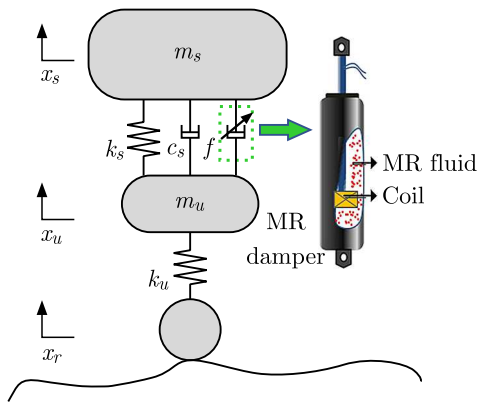

Fig. 1. Modeling of a semi-active suspension with MRD

The differential equations for semi-active suspension motion can be derived based on Newton's law of motion and Lagrange's law

$$\begin{aligned} &m_s\ddot{x}_s + c_s(\dot{x}_s - \dot{x}_u) + k_s(x_s - x_u) + f = 0 \\ &m_u\ddot{x}_u - c_s(\dot{x}_s - \dot{x}_u) - k_s(x_s - x_u) + k_u(x_u - x_r) - f = 0 \end{aligned} \tag{2.1}$$

In Eqs. (2.1), m_s and m_u are body mass and wheels mass, k_s is the suspension stiffness, x_s refers to the absolute displacement of vehicle body, c_s is the damping coefficient, x_r is the road surface excitation, k_t is the tire stiffness, x_u is the absolute displacement of the wheel, f stands for the damping force. The parameter values for the quarter semi-active suspension are shown Table 1.

Table 1. Parameter values of the quarter semi-active suspension

Parameter	Value	Unit
m_s	345	kg
m_u	40.5	kg
k_s	17	kN/m
k_u	192	kN/m
c_s	1500	Ns/m

To facilitate the design of the controller, the state is definined as

$$x_1 = x_s - x_u \qquad x_2 = \dot{x}_s \qquad x_3 = x_u - x_r \qquad x_4 = \dot{x}_u \tag{2.2}$$

The state-space equation is acquired form Eqs. (2.1) and (2.2) as follows

$$\dot{\mathbf{x}} = \mathbf{A}\mathbf{x} + \mathbf{B}f + \mathbf{C}\dot{x}_u \tag{2.3}$$

where

$$\mathbf{A} = \begin{bmatrix} 0 & -1 & 0 & -1 \\ -\dfrac{k_s}{m_s} & -\dfrac{c_s}{m_s} & 0 & \dfrac{c_s}{m_s} \\ 0 & 0 & 0 & 1 \\ \dfrac{k_s}{m_u} & \dfrac{c_s}{m_u} & -\dfrac{k_u}{m_u} & -\dfrac{c_s}{m_u} \end{bmatrix} \qquad \mathbf{B} = \begin{bmatrix} 0 \\ \dfrac{1}{m_s} \\ 0 \\ -\dfrac{1}{m_u} \end{bmatrix} \qquad \mathbf{C} = \begin{bmatrix} 0 \\ 0 \\ -1 \\ 0 \end{bmatrix}$$

2.2. Dynamic model of a magnetorheological damper

According to the modified Bouc-Wen model, this paper investigates MRD. Its structure includes a damping element, elastic element and hysteresis operator, as show in Fig. 2.

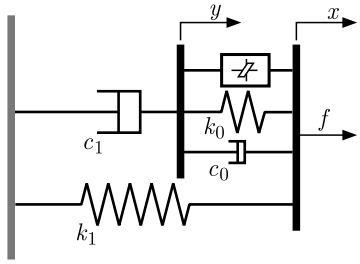

Fig. 2. Modified Bouc-wen model

The function expression is

$$\begin{aligned} &f = c_1\dot{y} + k_1(x - x_0) \qquad y = \frac{1}{c_0} + c_1[\delta z + c_0\dot{x} + k_0(x - y)] \\ &z = -\gamma|\dot{x} - \dot{y}|z|z|^{n-1} - \psi(\dot{x} - \dot{y})|z|^n + G(\dot{x} - \dot{y}) \end{aligned} \tag{2.4}$$

where c_1 and δ can be expressed as

$$c_1 = c_{1a} + c_{1b}\mathrm{i} \qquad \delta = \delta_a + \delta_b\mathrm{i} \tag{2.5}$$

In equations (2.4) and (2.5), x denotes the displacement of the spring, x_0 stands for the initial value, y is the internal displacement, c_0 represents viscous damping factor at a high speed, z is an evolutionary variable, k_0 stands for the stiffness coefficient, k_1 expresses the stiffness coefficient of the accumulator, c_1 represents the viscous damping factor at a low speed, δ indicates the scale factor of hysteresis operator, γ, ψ, n, G represent the adjustment coefficient.

3. Control system design

A novel control technique is developed utilizing the semi-active suspension of MRD. This technique incorporates the VUF-PID control model and the inverse model of MRD, which has been created using BPNN optimized with BWO, as depicted in Fig. 3.

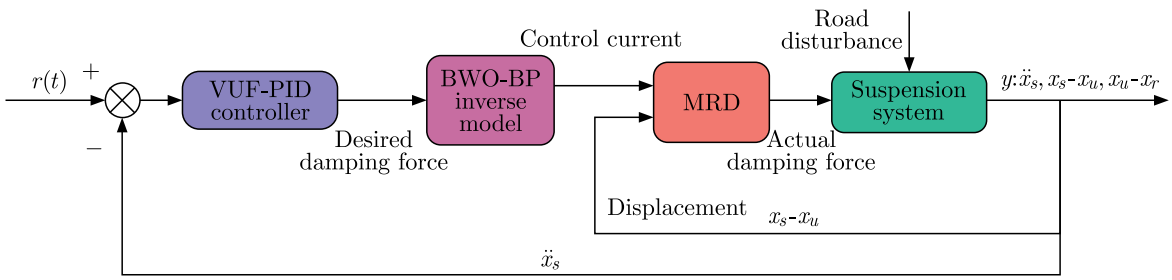

Fig. 3. Control schematic diagram

3.1. An inverse model of the magnetorheological damper

3.1.1. An inverse model based on BPNN

The BPNN is employed in constructing the inverse model of MRD, as depicted in Fig. 4. This figure also illustrates the correlation between the current and the damping force, as represented by the mapping relationship. Damping forces are obtained from the Modified Bouc-Wen model of magnetorheological dampers, the control current from random white noise, displacement of MRD data from suspension dynamic travel. 2000 sets of data were collected in total, with 1500 sets designated for network training and the remaining 500 sets reserved for testing purposes.

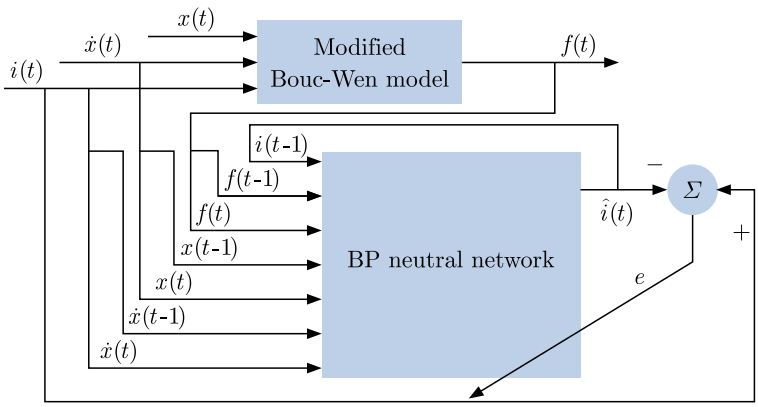

Fig. 4. Inverse model identification scheme of the MRD with BPNN

The neural network used in this study consists of three layers, namely the input layer, the hidden layer, and the output layer. It is composed of a total of seven input nodes, while the hidden layer comprises twelve nodes, and finally, a single output node. The inputs chosen for the neural network include the damping force, velocity, and displacement of MRD at time t and $t-1$, along with the control current at time $t-1$. The neural network output represents the current at time t.

3.1.2. Optimization of inverse models

During training, BPNN is likely to generate local optimum. In order to obtain more accurate current signals, this paper focuses on optimizing BPNN with the Beluga Whale Optimization (GWO). BWO, a bio-inspired optimization technique is applied to tackle challenging engineering and optimization issues. BPNN is most sensitive to weights and thresholds in initialization parameters. In the process of optimizing BPNN, BWO is equivalent to constantly updating the weights and thresholds and calculating the global optimum through multiple iterations. Figure 5 expresses the flow chart of the algorithm.

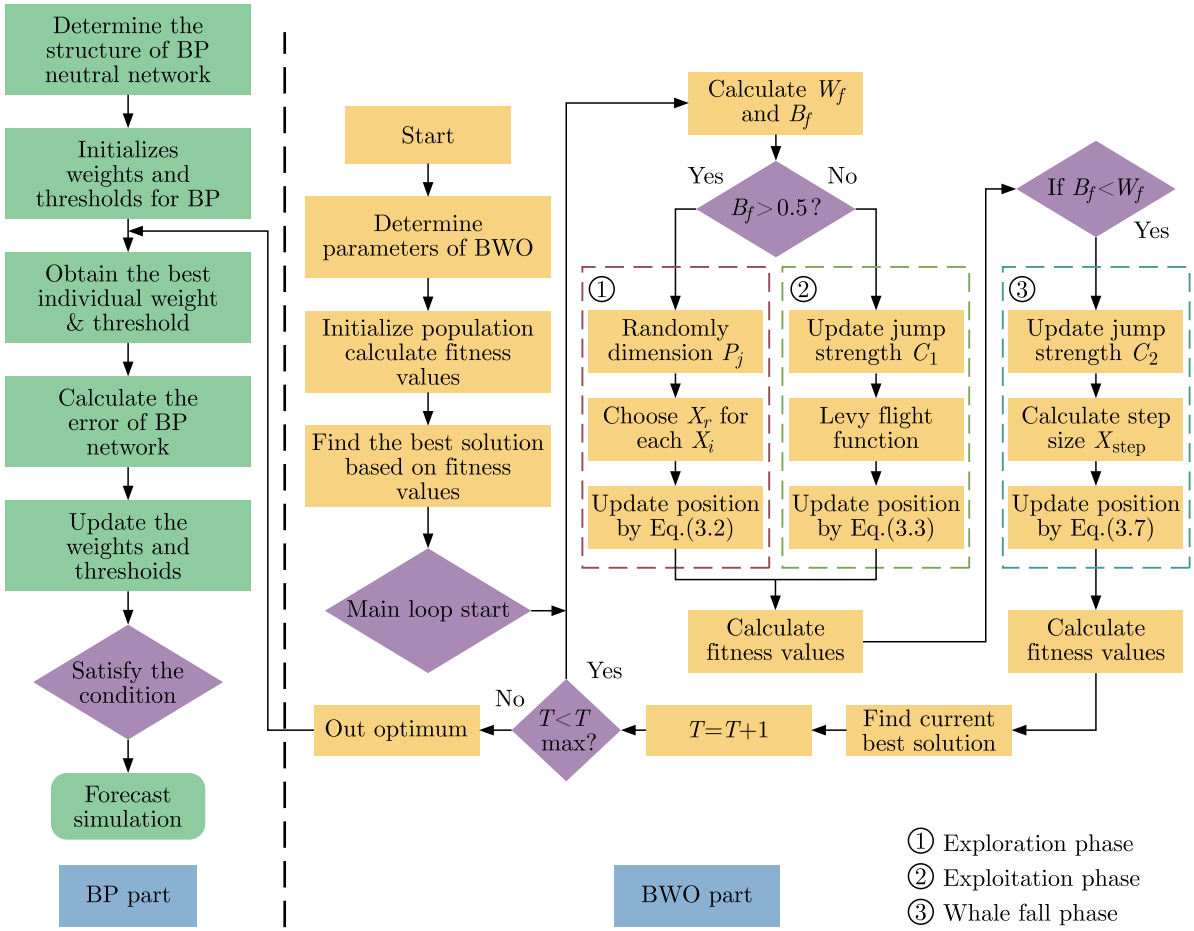

Fig. 5. The flow chart of BP neural network optimized by BWO

The main focus of this program lies in acquiring knowledge from the exploration and exploitation phases, as well as adopting behavioral traits observed in whales. In the BWO method, with the help of a balancing factor B_f, B_0 is randomly varied between $(0, 1)$ at each iteration. It allows conversion from exploration to exploitation. T and T_{max} denote the current and maximum number of iterations, respectively. The balance factor B_f can be expressed as

$$B_f = B_0\Big(1 - \frac{T}{2T_{max}}\Big) \tag{3.1}$$

When the B_f exceeds 0.5, the exploration phase commences, whereas when B_f falls below 0.5, it is the start of exploitation phase.

I) Exploration phase

Now, it is about to mimic beluga whales' swimming style. Depending on the odd and even numbers of positions, different positions are updated. Here is the mathematical model

$$x_{i,j}^{T+1} = \begin{cases} x_{r,P_j}^T + (x_{r,P_1}^T - x_{i,P_j}^T)(1+r_1)\sin(2\pi r_2) & \text{for} \quad j = \text{even} \\ x_{r,P_j}^T + (x_{r,P_1}^T - x_{i,P_j}^T)(1+r_1)\cos(2\pi r_2) & \text{for} \quad j = \text{odd} \end{cases} \tag{3.2}$$

where $x_{i,j}^{T+1}$ represents the i-th beluga whale in the j-th dimension, T denotes current iteration, r denotes randomly selected beluga whale. r_1 and r_2 indicate random numbers that range from 0 to 1, $\sin(2\pi r_2)$ and $\cos(2\pi r_2)$ denote mirrored beluga whales with their fins facing water.

II) Exploitation phase

The idea of this stage comes from the feeding behavior of beluga whales, which share information between themselves and their neighboring partners, so that the position of the best individual and other individuals can be updated. Introducing the Lévy flight strategy of predation, which is mathematically represented as

$$x_i^{T+1} = r_3 x_{best}^T - r_4 x_i^T + C_1 L_F (x_r^T - x_i^T) \tag{3.3}$$

where x_i^T stands for the i-th beluga whale's current position, x_r^T stands for random beluga whale's current positions, the optimal position for beluga whales is x_{best}^T, r_3 and r_4 indicate random numbers that range from 0 to 1, C_1 stands for the random jump strength used to gauge the Lévy flight intensity and represented by equation $(3.4)_1$, L_F represents the Lévy flight function, calculated from equation $(3.4)_2$

$$C_1 = 2r_4\Big(\frac{1-T}{T_{max}}\Big) \qquad L_F = 0.05\frac{u\sigma}{|v|^{1/\zeta}} \tag{3.4}$$

where u and v represent normally distributed random variables, while ζ represents a constant with a default value of 1.5σ, which is represented as

$$\sigma = \Big(\frac{\Gamma(1+\beta)\sin(\pi\zeta/2)}{\Gamma[(1+\beta)/2]\zeta 2^{(\zeta-1)/2}}\Big)^{1/\zeta} \tag{3.5}$$

III) Whale fall

Belugas face threats from orcas, polar bears and humans as they migrate and forage. The majority of belugas demonstrate their intelligence by evading these threats through effective communication. Nonetheless, some belugas unfortunately perish, sinking to depths of the ocean floor. This occurrence is referred to as a "whale fall".

In each iteration, to imitate the behavior of a whale fall, we simulate slight variations in the groups by selecting a likelihood of the whale fall from the individual. The beluga whales in question have either repositioned themselves or been subjected to expulsion and have subsequently descended into depths of the ocean. To establish the revised position, the utilization of beluga whale locations and the magnitude of their stride during falls is imperative. It guarantees the population size remain unaltered. The mathematical representation of the model is as follows

$$x_i^{T+1} = r_5 x_i^T - r_6 x + r_7 x_{step} \tag{3.6}$$

where r_5, r_6 and r_7 indicate a random numbers that range from 0 to 1, x_{step} indicates the step size for the whale fall, and x_{step} can be expressed as

$$x_{step} = (u_b - l_b)\exp\Big(-C_2\frac{T}{T_{max}}\Big) \tag{3.7}$$

where u_b represents the maximum limit of the variable, while l_b represents the minimum limit of the variable lower boundary. C_2 is expressed as

$$C_2 = 2W_f n \tag{3.8}$$

where C_2 denotes the step factor, W_f can be expressed as

$$W_f = 0.1 - 0.05\frac{T}{T_{max}} \tag{3.9}$$

As beluga whales progressively approach their source of sustenance, the level of risk associated with them diminishes throughout the optimization process. The evident proof arises from a drop in the likelihood of the whale fall, plunging from 0.1 in the initial iteration to 0.05 in the final iteration.

3.2. Control design of the suspension system

3.2.1. VUF-PID theory

The fuzzy PID controller integrates a variable universe controller known as VUF-PID. To enhance its performance, the fuzzy PID controller applies the expansion factor to incorporate the variable domain concept. The number of fuzzy rules at the local level is adjusted by this effect while overcoming the restricted accuracy caused by the limited count of fuzzy control rules found in the parameterization of the PID control problem. As shown in Fig. 6, the concept of fuzzy variable universe is aimed at changing the size of basic fuzzy variable set as the system error changes during the control process, thus ensuring dynamic adaptation for the optimized performance. In Fig. 6, x stands for input variables of the control system, μ represents the membership degree function, $\alpha(x)$ indicates the expansion factor of the input variable domain, e denotes the input initial domain.

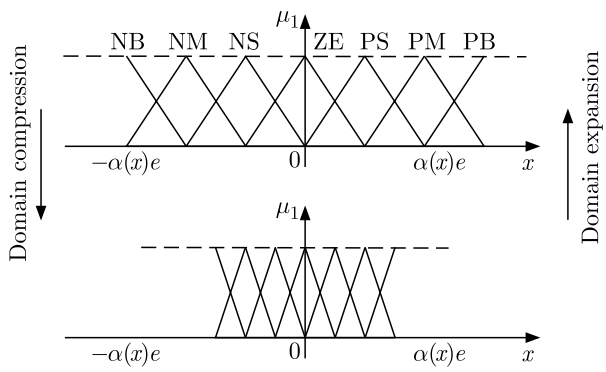

Fig. 6. Schematic diagram of universe transformation

3.2.2. Fuzzy PID controller

Figure 7 depicts the flow chart of fuzzy PID control, which builds upon the foundational PID control system through incorporation of fuzzy theory. This integration allows for the enhancement and improvement of the basic PID control approach. This paper adopts the two-input, three-output form of fuzzy control, controller inputs are error e and change rate of error ec. The error e is calculated as a difference between vertical acceleration of the vehicle $\ddot{x}_s$, and the set value $r(t) = 0$, ΔK_p, ΔK_i and ΔK_d as the controller output. The input and output variables are grouped into seven levels, denoted as NB, NM, NS, ZE, PS, PM, PB. All domains have a range of $(-6, 6)$ configured. The triangle function is employed for the membership functions of input and output. Fuzzy inference rules are established based on the suspension system characteristics, displayed in Table 2.

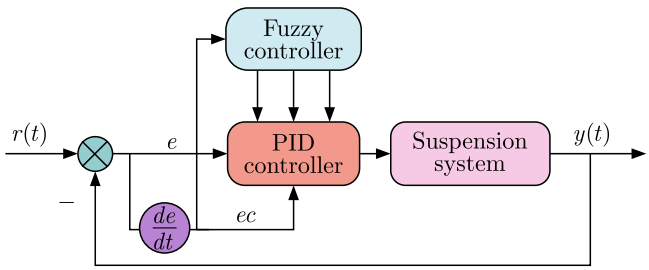

Fig. 7. Fuzzy-PID controller scheme

Table 2. Fuzzy rule table

	NB	NM	NS	ZE	PS	PM	PB
NB	PB/NB/PS	PB/NB/NS	PM/NM/NB	PM/NM/NB	PS/NS/NB	ZE/ZE/NM	ZE/ZE/PS
NM	PB/NB/PS	PB/NB/NS	PM/NM/NB	PM/NS/NM	PS/NS/NM	ZE/ZE/NS	NS/ZE/ZE
NS	PM/NM/ZE	PM/NM/NS	PM/NS/NM	PS/NS/NM	ZE/ZE/NS	NS/PS/NS	NS/PS/ZE
ZE	PM/NM/ZE	PM/NM/NS	PS/NS/NS	ZE/ZE/NS	NS/PS/NS	NM/PM/NS	NM/PM/ZE
PS	PS/NM/ZE	PS/NS/ZE	ZE/ZE/ZE	NS/PS/ZE	NS/PS/ZE	NM/PM/ZE	PM/PB/ZE
PM	PS/ZE/PB	ZE/ZE/NS	NS/PS/PS	NM/PS/PS	NM/PM/PS	NM/PB/PS	NB/PB/PB
PB	ZE/ZE/PB	ZE/ZE/PM	NM/PS/PM	NM/PM/PM	NM/PM/PS	NB/PB/PS	NB/PB/PB

Based on the control principle of fuzzy PID, the formula for adjusting the parameters of PID is presented below

$$K_p = K_{p0} + \Delta K_p \qquad K_i = K_{i0} + \Delta K_i \qquad K_d = K_{d0} + \Delta K_d \tag{3.10}$$

3.2.3. VUF-PID controller

In variable universe fuzzy control, the expansion factor directly determines the precise control effect and overall control performance. The universe formula for the scaling factor is as follows

$$X_e = [-\alpha e, \alpha e] \qquad Y = [-\beta u, \beta u] \tag{3.11}$$

where α, β can be regarded as the scaling factors for input and output, e, u represent the original input and output universe, X_e, Y denote the resultant input and output universe.

The present investigation utilizes the VUF-PID function (Zeng *et al.*, 2020), as depicted in Fig. 8. The scaling coefficients primarily derived from functional models are produced via functions parameterized by the error and its rate of change. The scaling factors change in the form of exponent

$$\alpha(x) = 1 - \lambda \mathrm{e}^{-kx^2} \qquad \beta(t) = K_I \sum_{i=1}^{n} P_i \int_0^t e_i(\tau)\, d\tau + \beta(0) \tag{3.12}$$

In Eq. (3.12), $9 < \lambda < 1$, $k > 0$, the value of k reflects changing speed of universe of the controller, λ reflects accuracy of the controller, K_I, P_i are constants, $\beta(0)$ is the initial value, $e_i(\tau)$ is the error vector, τ is the adjustment parameter.

The domain of the input variable is

$$X_e(e) = [-\alpha(x)e, \alpha(x)e] \qquad X_e(ec) = [-\alpha(x)ec, \alpha(x)ec] \tag{3.13}$$

Based on the characteristics of MRD semi-active suspension, taking into account the influence of parameters λ and k in the scaling factor, based on experience and after multiple experiments, the value of λ is 0.6 and k is 0.5, then

$$\alpha(e) = 1 - 0.6\mathrm{e}^{-0.5e^2} \qquad \alpha(ec) = 1 - 0.6\mathrm{e}^{-0.5ec^2} \tag{3.14}$$

The variation of integral coefficient K_i tends to opposite direction to the variation of the system deviation, whereas the variation of the output variables K_p and K_d are consistent with variation of the system deviation. The following are the scaling factors for K_p, K_i and K_d

$$\beta(K_p) = 3|e| \qquad \beta(K_i) = \frac{1}{|e| + 0.9} \qquad \beta(K_d) = 3|e| \tag{3.15}$$

The changed output variables $Y(K_p)$, $Y(K_p)$ and $Y(K_d)$ domains can be expressed as

$$\begin{aligned} &Y(K_p) = [-\beta(K_p)K_p, \beta(K_p)K_p] \qquad Y(K_i) = [-\beta(K_i)K_i, \beta(K_i)K_i] \\ &Y(K_d) = [-\beta(K_d)K_d, \beta(K_d)K_d] \end{aligned} \tag{3.16}$$

The fuzzy tuning relation is defined by Θ, the output of the fuzzy control is

$$\begin{aligned} &\Delta K_p = \Theta[\beta(K_p)\Theta(\alpha(x)e, \alpha(x)ec)] \qquad \Delta K_i = \Theta[\beta(K_i)\Theta(\alpha(x)e, \alpha(x)ec)] \\ &\Delta K_d = \Theta[\beta(K_d)\Theta(\alpha(x)e, \alpha(x)ec)] \end{aligned} \tag{3.17}$$

In summary, the output of the controller is

$$f(k) = (\Delta K_p + K_{p0})e(k) + (\Delta K_i + K_{i0})\int_0^k e(k)\,dk + (\Delta K_d + K_{d0})\frac{de(k)}{dk} \tag{3.18}$$

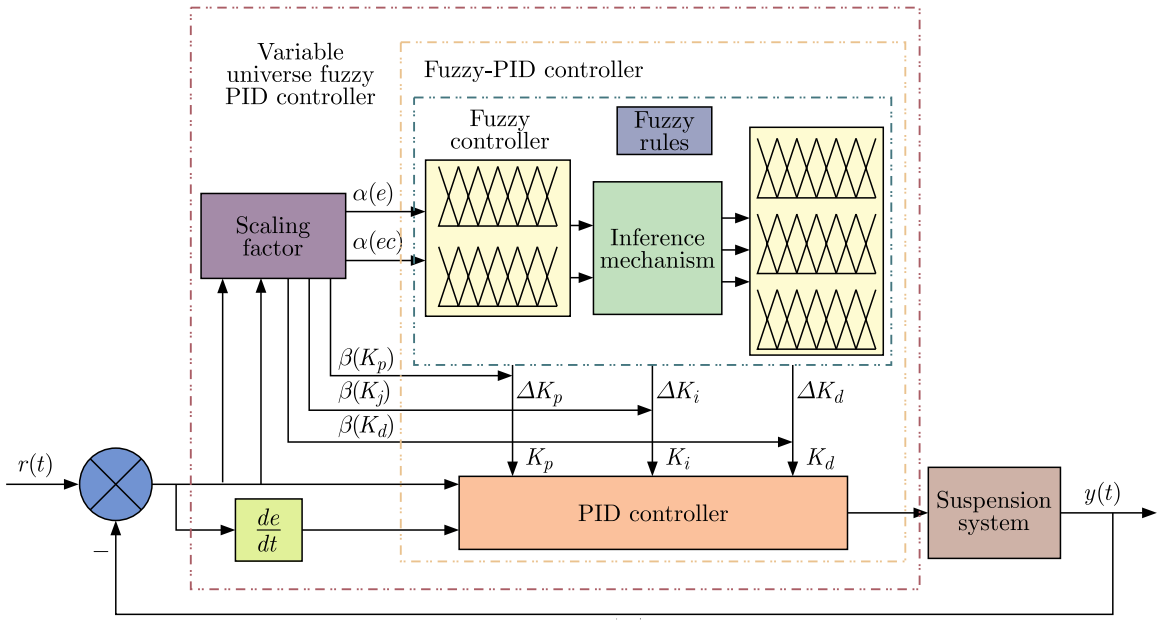

Fig. 8. Variable universe fuzzy PID control system

4. Simulation analysis

4.1. Performance of MRD

According to Eqs. (2.4) and (2.5), the model of MRD is established. Table 3 displays the research parameters for the Bouc-Wen phenomenon model (Sosthene *et al.*, 2018). The displacement follows a sinusoidal pattern with 10mm amplitude and 2Hz frequency, while the current ranges from 0A, 1A, 2A to 3A. Figure 9 illustrates the property of MRD divided into three portions for description, which included the force-time curve, force-displacement curve and force-velocity curve.

To assess the efficacy of the BWO, comparison and analysis of the prediction results of the inverse model built by BPNN before and after optimization are made. Figure 10a illustrates the original current and predictive control current with BPNN and BWO-BPNN, in Fig. 10b, a comparison is displayed between the control current of the BPNN and the BWO-BPNN, highlighting the errors. Based on the comparison of prediction results and errors provided by

Table 3. Bouc-Wen model parameters (Sosthene *et al.*, 2018)

Parameter	Value	Parameter	Value
C_0 [Ns/m]	997	k_1 [–]	134
C_{1a} [Ns/(mA)]	8186	x_0 [–]	0.115
C_{1b} [Ns/(mA)]	2725	ψ [m^2]	70000
δ_a [N/m]	0	G [–]	300
δ_b [N/m]	1723	γ [1/m^2]	70000
k_0 [–]	1072	n [–]	2

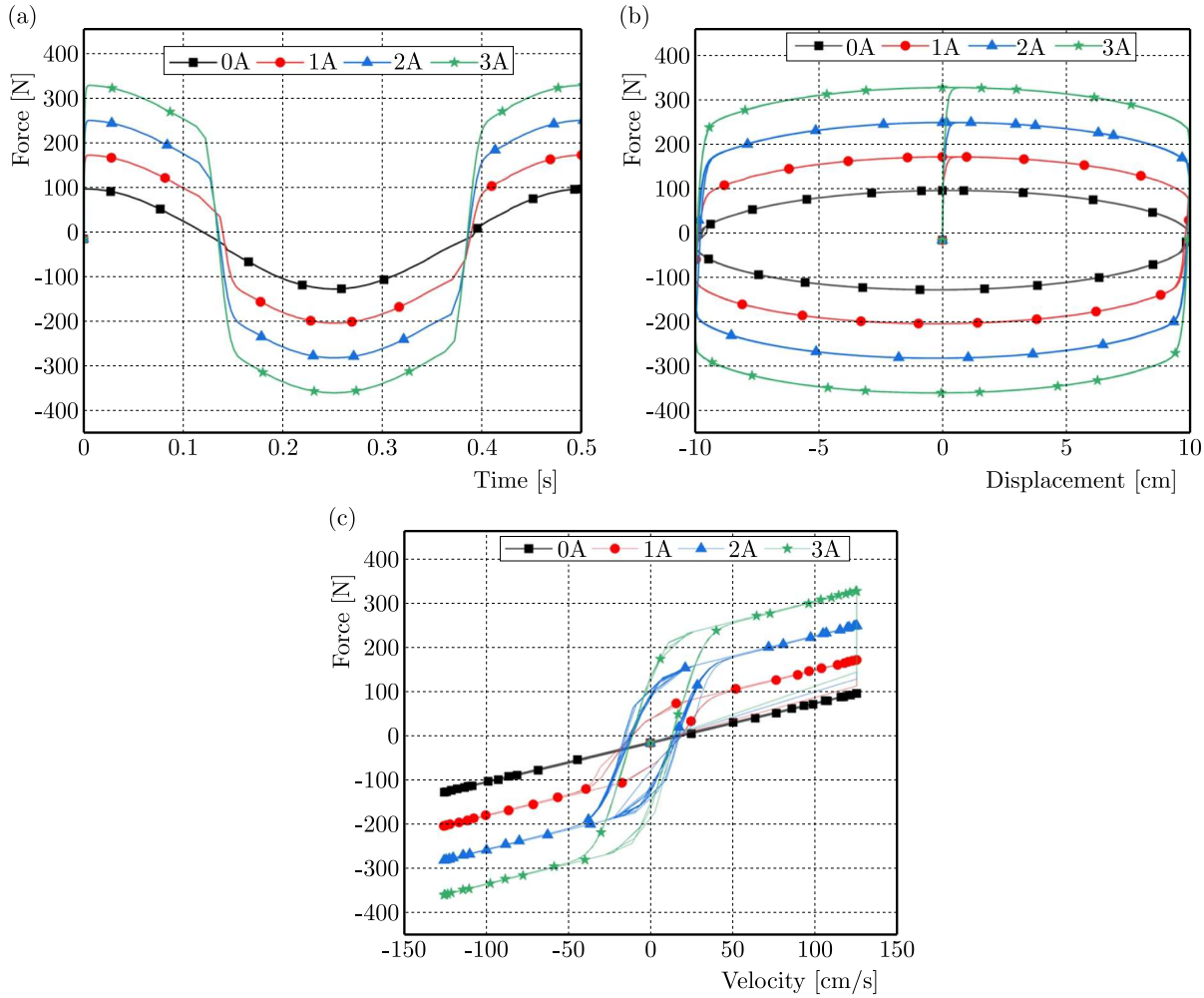

Fig. 9. Performance of MRD with different applied currents: (a) force versus time curve, (b) force versus displacement curve, (c) force versus velocity curve

Fig. 10, it is seen that BWO-BPNN has a superior fitting results of the control current predicted to original current sample than that of BPNN. Moreover, the root mean square (RMS) value of BWO-BPNN prediction error is smaller than that of BPNN, with RMS value of 0.0025621 and BPNN of 0.006093. In addition, the BWO-BPNN fitting error is reduced by 57.97%, which demonstrates the superior performance of the inverse model by BWO-BPNN.

4.2. Performance of the system controller

With the aim at thoroughly assessing the effectiveness of this controller, two types of road excitation random and sinusoidal are introduced.

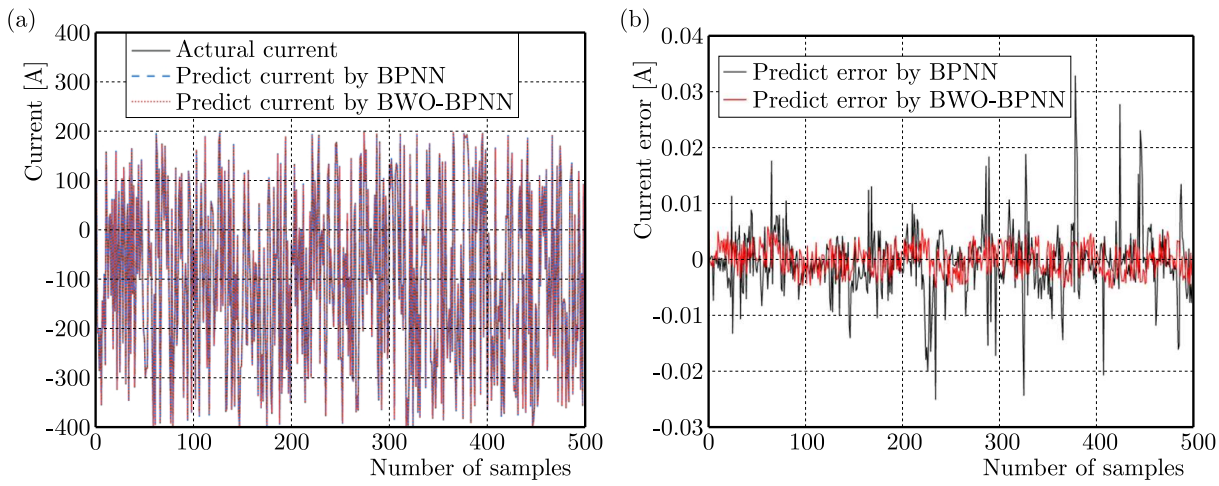

Fig. 10. The predicted values of the current using the BWO-BP and BPNN: (a) current, (b) current error

4.2.1. Random road

The random road is created by white noise. The model expression is

$$\dot{q}_t = -2\pi f_{min} q_t + 2\pi n_0 \sqrt{Gq(n_0)} W_t \tag{4.1}$$

where $\dot{q}_t$ is the impact strength, f_{min} is the time frequency, n_0 denotes the spatial frequency, $G_q(n_0)$ stands for the road unevenness coefficient, v is the travel speed, W_t expresses the Gaussian white noise. In this simulation: $v = 40\,\mathrm{m/s}$, $G_q(n_0) = 64 \cdot 10^{-6}\,\mathrm{m/s}$, $n_0 = 0.1\,\mathrm{m}^{-1}$.

Figure 11 interprets variation of the suspension performance under a random surface. In this investigation, a comparison is made between four distinct suspension systems, namely passive suspension, fuzzy control, fuzzy PID control, and VUF-PID control. Performance in the time and frequency domain is analyzed to evaluate their respective effectiveness. Figures 11a,b represent body vertical acceleration, by making use of VUF-PID. The body vertical acceleration is effectively reduced, improving riding comfort. Figures 11c,d indicate the suspension dynamic displacement, VUF-PID control reduces its value to avoid the breakdown phenomenon. The stability of the vehicle is ensured by VUF-PID control, as demonstrated in Figs. 11e,f, which depicts the dynamic load on the wheel. According to the frequency domain results, the VUF-PID controller has the best results in the low frequency range of 0-20 Hz.

Table 4 displays RMS values of the suspension performance index for various control methods employed on the random road surface. Compared to the passive suspension, the vehicle body experiences a decrease in vertical acceleration by 15.85%, 36.21%, and 41.29%, while the suspension deflects dynamically by 5.57%, 33.44%, and 37.70%, respectively. Additionally, the dynamic load on the wheel witnesses a reduction of 4.01%, 35.02%, and 40.46% correspondingly.

Table 4. Simulation results under the random road

Control method	Performance indicators		
	body vertical acceleration [m/s^2]	suspension dynamic travel [m]	wheel dynamic load [N]
Passive	0.322836	0.008760	183.2071
Fuzzy	0.271669	0.008272	175.8765
Fuzzy-PID	0.205912	0.005831	119.0387
VUF-PID	0.189534	0.005458	109.0793

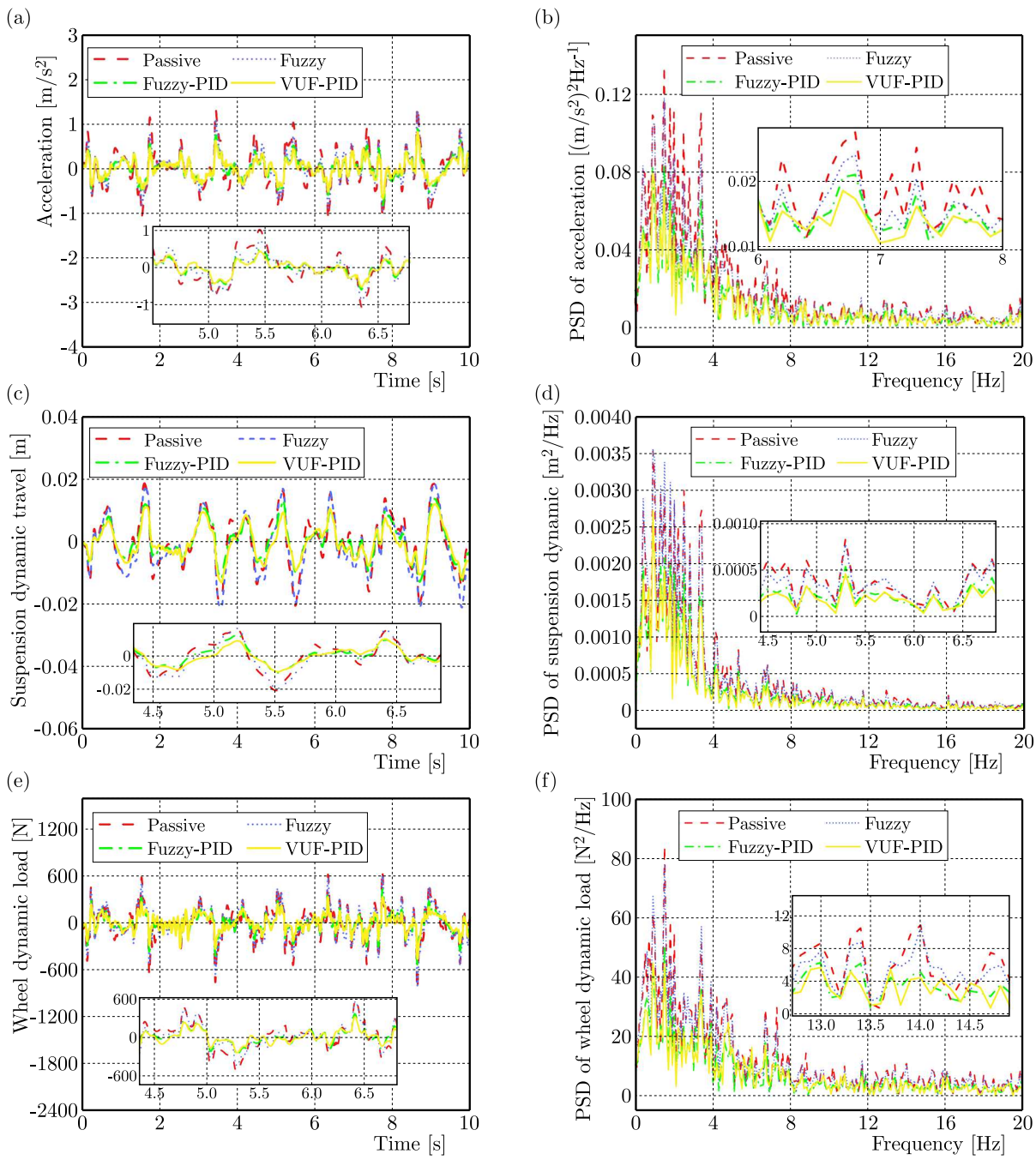

Fig. 11. Performance indexes of different control under the random road suspension system: (a) body vertical acceleration (time domain), (b) body vertical acceleration (frequency domain), (c) suspension dynamic travel (time domain), (d) suspension dynamic travel (frequency domain), (e) wheel dynamic load (time domain), (f) wheel dynamic load (frequency domain)

4.2.2. Sinusoidal road

The second road model is adopted: a sinusoidal road surface. A sinusoidal road signal is a common road excitation for suspension vibration analysis. Its is model expression is

$$x_r = \xi \sin(\omega x) \tag{4.2}$$

where ξ [m] represents the road displacement, ω [rad/s] represents the angular frequency. In this simulation, the road displacement is 0.02 m and the angular frequency is 4π rad/s.

Figure 12 shows the variation of suspension performance index under the sinusoidal road signal. The performance measures of the suspension system are enhanced when comparing it to the passive suspension through implementations of fuzzy control, fuzzy PID control, and VUF-PID control.

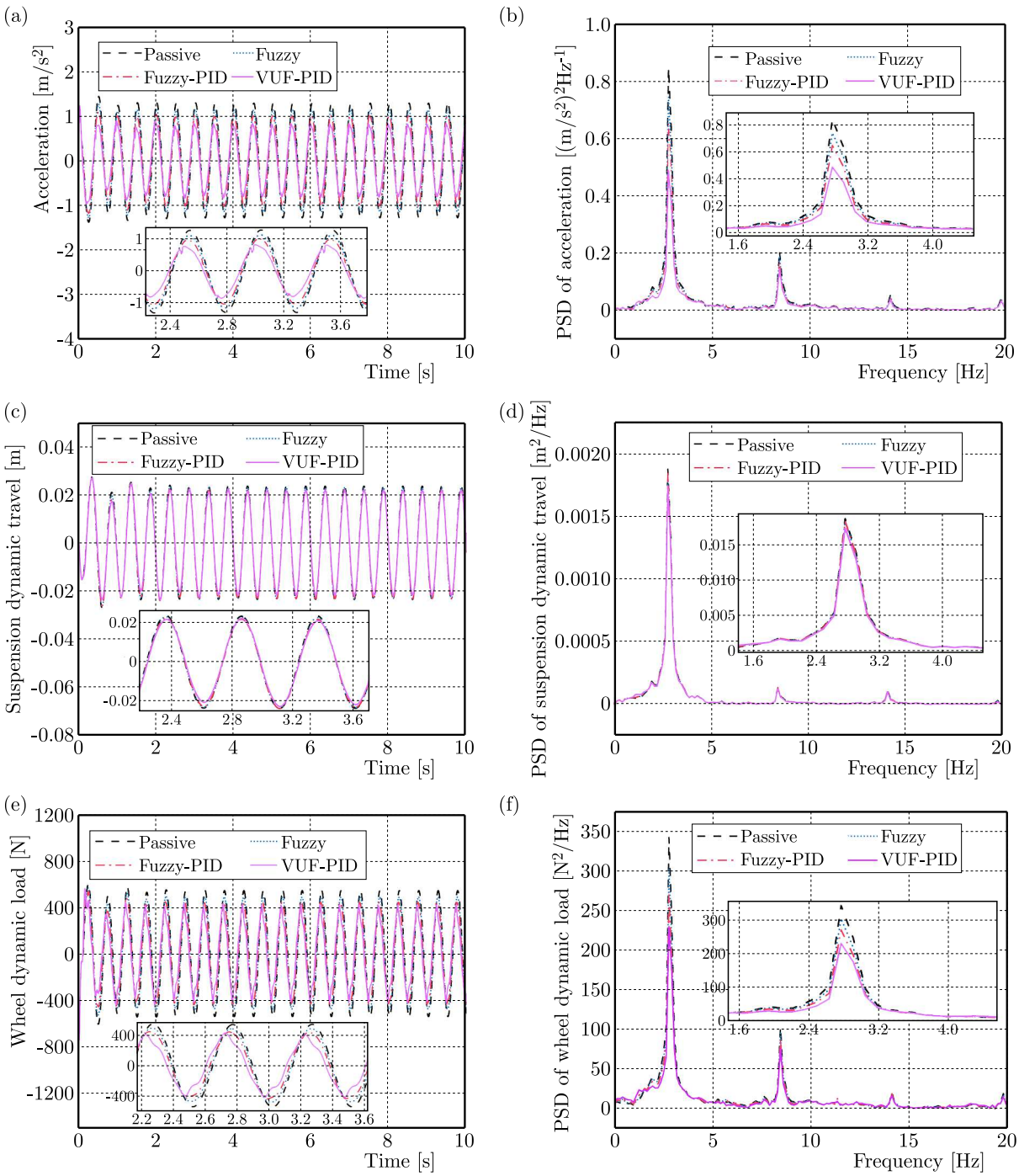

Fig. 12. Performance indexes of different control under the sinusoidal road suspension system: (a) body vertical acceleration (time domain), (b) body vertical acceleration (frequency domain), (c) suspension dynamic travel (time domain), (d) suspension dynamic travel (frequency domain), (e) wheel dynamic load (time domain), (f) wheel dynamic load (frequency domain)

Table 5 shows the RMS values of the suspension performance index across different control strategies when subjected to a sinusoidal road surface. In comparison to the passive suspension,

the vehicle body experiences a reduction in vertical acceleration by 11.46%, 22.12%, and 39.90%, while the suspension dynamic deflection decreases by 1.88%, 3.67%, and 7.04% correspondingly. Additionally, there is a consecutive decrease in the dynamic load observed for the wheel by 10.47%, 19.39%, and 29.28%.

Table 5. Simulation results under the sinusoidal road

Control method	Performance indicators		
	body vertical acceleration [m/s^2]	suspension dynamic travel [m]	wheel dynamic load [N]
Passive	0.845642	0.018207	344.8268
Fuzzy	0.748745	0.017864	308.722
Fuzzy-PID	0.658616	0.017539	277.9482
VUF-PID	0.508267	0.016926	243.8728

5. Conclusions

In this study, a functional VUF-PID control is developed with a quarter magnetorheological semi-active suspension system. In the semi-active suspension control system with MRD, the damping effect depends not only on the control algorithm of the system, but also on the precise mechanical model of MRD.

- The modified Bouc-Wen model of MRD is created, and the relationship between the damping force and displacement as well as velocity under different control currents is analyzed, which shows accurate characteristics of MRD. By using the BWO-BPNN to create an inverse model of the MRD, the fitting error has decreased by 57.97%, and the output prediction current has been more accurate compared with the BPNN.
- In this study, a functional VUF-PID control is developed with a quarter magnetorheological semi-active suspension system. With the additional control methods stated in this research, the performance indices of the suspension improved under different conditions (random road, sinusoidal road). The controller is better suited and more efficient.

Acknowledgments

The authors research is supported by Liaoning Provincial Department of Education Basic Research Project (Project No. LJKMZ20220602) and 2021 Scientific research support for high-level talent from Shenyang Ligong University (1010147001001).

References

1. Al Aela A.M., Kenne J.-P., Mintsa H.A., 2022, Adaptive neural network and nonlinear electrohydraulic active suspension control system, *Journal of Vibration and Control*, **28**, 3-4, 243-259

2. Boada M.J.L., Boada B.L., Diaz V., 2018, A novel inverse dynamic model for a magnetorheological damper based on network inversion, *Journal of Vibration and Control*, **24**, 15, 3434-3453

3. Chen K.Y., 2022, A new state observer-based vibration control for a suspension system with magnetorheological damper, *Vehicle System Dynamics*, **60**, 9, 3127-3150

4. Dong X., Yu M., Liao C., Chen W., 2010, Comparative research on semi-active control strategies for magneto-rheological suspension, *Nonlinear Dynamics*, **59**, 3, 433-453

5. Gong M., Chen H., 2020, Variable damping control strategy of a semi-active suspension based on the actuator motion state, *Journal of Low Frequency Noise, Vibration and Active Control*, **39**, 3, 787-802
6. Krzyzynski T., Maciejewski I., 2019, Computational method for shaping the vibro-isolation properties of semi-active and active systems, *Archives of Mechanics*, **71**, 4-5, 291-313
7. Liu P., Zheng M., Ning D., Zhang N., Du H., 2022, Decoupling vibration control of a semi--active electrically interconnected suspension based on mechanical hardware-in-the-loop, *Mechanical Systems and Signal Processing*, **166**, 108455
8. Lou Z., Ervin R.D., Filisko F.E., 1994, A preliminary parametric study of electrorheological dampers, *Journal of Fluids Engineering*, **116**, 3, 570-576
9. Ma T., Bi F., Wang X., Tian C., Lin J., *et al.*, 2021, Optimized fuzzy skyhook control for semi--active vehicle suspension with new inverse model of magnetorheological fluid damper, *Energies*, **14**, 6, 1674
10. Maciejewski I., Krzyzynski T., Pecolt S., Chamera S., 2019, Semi-active vibration control of horizontal seat suspension by using magneto-rheological damper, *Journal of Theoretical and Applied Mechanics*, **57**, 2, 411-420
11. Mai V.N., Yoon D.-S., Choi S.-B., Kim G.-W., 2020, Explicit model predictive control of semi--active suspension systems with magneto-rheological dampers subject to input constraints, *Journal of Intelligent Material Systems and Structures*, **31**, 9, 1157-1170
12. Morales A.L., Nieto A.J., Chicharro J.M., Pintado P., 2018, A semi-active vehicle suspension based on pneumatic springs and magnetorheological dampers, *Journal of Vibration and Control*, **24**, 4, 808-821
13. Muthalif A.G.A., Kasemi H.B., Nordin N.H.D., Rashid M.M., Razali M.K.M., 2017, Semi-active vibration control using experimental model of magnetorheological damper with adaptive F-PID controller, *Smart Structures and Systems*, **20**, 1, 85-97
14. Na J., Huang Y., Wu X., Liu Y.-J., Li Y., Li G., 2022, Active suspension control of quarter--car system with experimental validation, *IEEE Transactions on Systems, Man, and Cybernetics: Systems*, **52**, 8, 4714-4726
15. Na J., Huang Y., Wu X., Su S.-F., Li G., 2020, Adaptive finite-time fuzzy control of nonlinear active suspension systems with input delay, *IEEE Transactions on Cybernetics*, **50**, 6, 2639-2650
16. Pang H., Liu F., Xu Z., 2018, Variable universe fuzzy control for vehicle semi-active suspension system with MR damper combining fuzzy neural network and particle swarm optimization, *Neurocomputing*, **306**, 130-140
17. Papaioannou G., Koulocheris D., Velenis E., 2021, Skyhook control strategy for vehicle suspensions based on the distribution of the operational conditions, *Proceedings of the Institution of Mechanical Engineers, Part D: Journal of Automobile Engineering*, **235**, 10-11, 2776-2790
18. Shin D.K., Phu D.X., Choi S.M., Choi S.B., 2016, An adaptive fuzzy sliding mode control of magneto-rheological seat suspension with human body model, *Journal of Intelligent Material Systems and Structures*, **27**, 7, 925-934
19. Sosthene K., Josee M., Xiong H., 2018, Fuzzy logic controller for semi active suspension based on magneto-rheological damper, *International Journal of Automotive Engineering and Technologies*, **7**, 1, 38-47
20. Tang X., Ning D., Du H., Li W., Wen W., 2020, Takagi-Sugeno fuzzy model-based semi-active control for the seat suspension with an electrorheological damper, *IEEE Access*, **8**, 98027-98037
21. Trikande M.W., Karve N.K., Anand Raj R., Jagirdar W., Vasudevan R., 2018, Semi--active vibration control of an 8x8 armored wheeled platform, *Journal of Vibration and Control*, **24**, 2, 283-302
22. Tseng H.E., Hrovat D., 2015, State of the art survey: active and semi-active suspension control, *Vehicle System Dynamics*, **53**, 7, 1034-1062

23. Wang W., Song Y., Xue Y., Jin H., Hou J., Zhao M., 2015, An optimal vibration control strategy for a vehicle's active suspension based on improved cultural algorithm, *Applied Soft Computing*, **28**, 167-174

24. Zeng W., Jiang Q., Xie J., Yu T., 2020, A functional variable universe fuzzy PID controller for load following operation of PWR with the multiple model, *Annals of Nuclear Energy*, **140**, 107174

25. Zhang B., Zhao H., Zhang X., 2024, Adaptive variable domain fuzzy PID control strategy based on road excitation for semi-active suspension using CDC shock absorber, *Journal of Vibration and Control*, **30**, 3-4, 860-875

26. Zhang N., Zhao Q., 2017, Fuzzy sliding mode controller design for semi-active seat suspension with neuro-inverse dynamics approximation for MR damper, *Journal of Vibroengineering*, **19**, 5, 3488-3511

27. Zhong C., Li G., Meng Z., 2022, Beluga whale optimization: A novel nature-inspired metaheuristic algorithm, *Knowledge-Based Systems*, **251**, 109215

Manuscript received November 7, 2023; accepted for publication September 19, 2024